Soft Matter

Positional Ordering Induced by Dynamic Steric Interactions in Superparamagnetic Rods

Journal:	*Soft Matter*
Manuscript ID	SM-ART-11-2022-001519.R2
Article Type:	Paper
Date Submitted by the Author:	05-Jan-2023
Complete List of Authors:	Brisbois, Chase; Northwestern University, Materials Science and Engineering Olvera de la Cruz, Monica; Northwestern University, Materials Science and Engineering

ARTICLE

Positional Ordering Induced by Dynamic Steric Interactions in Superparamagnetic Rods

Received 00th January 20xx,
Accepted 00th January 20xx

DOI: 10.1039/x0xx00000x

Chase Austyn Brisbois,[a] and Monica Olvera de la Cruz*[a,b,c]

The dynamic motion produced by precessing magnetic fields can drive matter into far-from-equilibrium states. We predict 1D periodic ordering in systems of precessing rods when magnetic interactions between rods remain insignificant. The precession angle of the rods is completely determined by the field's precession angle and the ratio of the field's precession frequency and the characteristic response frequency of the rods. We develop a molecular dynamics model that explicitly calculates magnetic interactions between particles, and we also simulate rods in the limit of a strong and fast precessing magnetic field where inter-rod magnetic interactions are negligible, using a purely steric model. Our simulations show how steric interactions drive the rods from a positionally disordered phase (nematic) to a layered (smectic) phase. As the rod precession angle increases, the nematic-smectic transition density significantly decreases. The minimization of unfavorable steric interactions also induces phase separation in binary mixtures of rods of different lengths. This effect is general to any force that produces precession in elongated particles. This work will advance the understanding and control of out-of-equilibrium soft matter systems.

1 Introduction

Colloidal crystals composed of superparamagnetic particles are shown as promising platforms for optoelectronics,[1,2] mechanosensors,[3] and filtration[4,5] devices due to their biocompatibility and responsiveness. By this nature, externally applied magnetic fields control the morphological evolution of the crystal.[6,7,8] While crystalline ordering is usually driven by close-packing,[9,10] chemical bonds,[11,12] or magnetic interactions,[13,14] it can also be controlled by particle shape and motion.[15] Such entropic effects emerge when thermal energy is significant allowing non-spherical particles to adopt liquid crystal phases.[16]

Spontaneous 1D positional ordering arises from collections of elongated particles (the so-called smectic phase), whereby they develop a layered structure.[15] Smectic liquid crystals have many applications in science and technology such as optical films,[17] electromechanical sensors,[18] actuators,[19] and fabrication platforms,[20] owed to this layered 1D period order. It even has an emerging relevance in cell biology.[21] Magnetic fields can guide the formation of the smectic phase for systems where the magnetic interactions between particles is weak.[22]

Interactions between superparamagnetic particles can be estimated by calculating the magnetic coupling constant[23] $\Gamma = \mu_o\mu^2/2\pi d^3 k_B T$, where μ_o is the magnetic constant, μ is the dipole magnitude, k_B is the Boltzmann constant, T is the absolute temperature, and d is the distance between dipoles. It represents the strongest possible magnetic interaction relative to thermal energy. If $\Gamma \gg 1$, magnetic interactions dominate over thermal forces and the system can become fixed in a magnetic-stabilized state. New physics can be uncovered by studying systems where $\Gamma \ll 1$. In this regime, the magnetic field manipulates the motion of the particles and the small Γ prevents aggregation or repulsive trapping.[24] Magnetic particles are often coated in a non-magnetic layer to act as a linking agent, biocompatibility layer, and an aggregation inhibitor.[25,26] Additionally, by operating in a low magnetic coupling regime, the applicability of results is expanded to any system that generates a field or force (electrical, chemical or hydrodynamic) that produces similar particle motion.

In this paper, we use a combination of theory and molecular dynamics models to demonstrate how a precessing magnetic field can drive a system of coated (low Γ) superparamagnetic rods into the smectic phase. First, we describe the motion of the rods using theory and define the valid regime for the purely steric "strong precession" molecular dynamics (MD) model that forgoes the need for explicit magnetic calculations. Next, we explain that the system is defined by two parameters: the reduced concentration ρd^3, and the rod precession angle β. On this phase diagram, we compare simulations using explicit magnetic calculations to the steric MD model and see how both show larger β favours the smectic phase. Finally, we demonstrate how rod interaction drives phase separation in binary mixtures.

[a] a Department of Materials Science and Engineering, Northwestern University, Evanston, IL 60208, USA.
[b] b Department of Chemistry, Northwestern University, Evanston, IL 60208, USA.
[c] c Department of Physics and Astronomy, Northwestern University, Evanston, IL 60208, USA.
* Corresponding author.
Electronic Supplementary Information (ESI) available: [details of any supplementary information available should be included here]. See DOI: 10.1039/x0xx00000x

2 Model

We seek to predict the nematic-smectic phase transition in a system of precessing superparamagnetic rods. The rods are composed of a linear chain of superparamagnetic particles that are coated in a non-magnetic material that forms a rigid shell (e.g. silica).[27] To this end, we begin by calculating the precession angle of the rod β. While this angle is suppressed at very high densities, this investigation will inform how the phase diagram can be constructed. Then, we will describe a purely steric MD model that forgoes the need for costly magnetic calculations. Finally, we will describe the "full" MD model against which our other models can be tested.

2.1 Precession angle for dilute superparamagnetic rods

An externally applied magnetic field controls the orientation of superparamagnetic rods. The orientation of the rod is parametrized by the angle with respect to the precession axis β and the azimuthal angle α. By convention, we align the precession axis in the z-direction and measure the azimuthal angle from the x-axis. We apply a precessing magnetic field in the direction $\hat{\boldsymbol{H}} = (\sin\theta\cos\omega t, \sin\theta\sin\omega t, \cos\theta)$, where θ is the magnetic field precession angle, ω is the precession angular frequency, and t is time. For a superparamagnetic system, $\boldsymbol{H} = \boldsymbol{\mu}/\chi$, where χ is the magnetic susceptibility and $\boldsymbol{\mu}$ is the dipole moment. When switching between materials with different magnetic susceptibilities, the dipole can remain constant by modulating the field strength. For $\cos\theta < 1/\sqrt{3}$, a stiff rod will precess synchronous to the field and avoid oscillatory behaviour.[28] Therefore, we define the orientation of the rod using its long axis, $\hat{\boldsymbol{n}} = (\sin\beta\cos\alpha, \sin\beta\sin\alpha, \cos\beta)$, where β is the angle from the z-axis, and $\alpha = \omega t - \phi$, where ϕ is the phase lag.

The phase lag determines the magnetic torque acting on the superparamagnetic rod and must be balanced by the drag torque. We define the drag torque according to a Rayleigh viscous dissipation function P added to the Euler-Lagrange (EL) equation,[29]

$$\frac{d}{dt}\frac{\partial L}{\partial \dot{\alpha}} - \frac{\partial L}{\partial \alpha} + \frac{\partial P}{\partial \dot{\alpha}} = 0. \quad (1)$$

Where $\dot{\alpha} = d\alpha/dt$, and $L = T - U$ is the Lagrangian, where T is the kinetic energy and U is the potential energy. In a manner similar to previous work on magnetoelastic membranes,[30] the EL equation is constructed from the interactions of superparamagnetic particles moving in a viscous fluid. Furthermore, in a Stokes regime, acceleration terms can be neglected leaving us with the simple form

$$\frac{\partial U}{\partial \alpha} + \frac{\partial P}{\partial \dot{\alpha}} = 0. \quad (2)$$

The rods do not stretch or bend so only the magnetic interactions contribute to the potential energy U. We use a nearest neighbours approach to calculate the dipole-dipole interactions of each superparamagnetic particle. Each dipole is identical in strength and orientation leading to

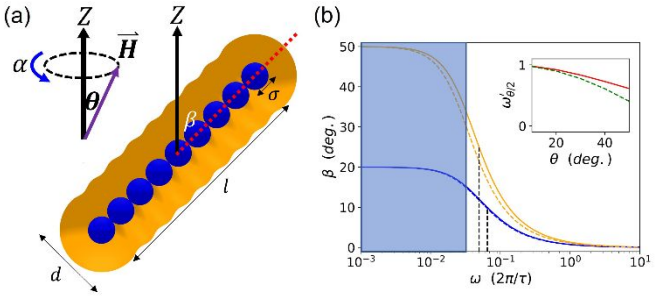

Fig. 1 Precession of a superparamagnetic rod. (a) Schematic for a magnetic field $\boldsymbol{H}$ precessing around the z-axis at a precession angle θ. A rod composed of a stiff chain of superparamagnetic particles (blue) of diameter σ are coated by a non-magnetic material (orange); the coating determines its aspect ratio l/d. The rod orientation is measured by its angle β to the precession (z) axis. (b) The external field $\boldsymbol{H}$ drives rod precession for $\theta = 20°$ and $50°$. As the field precession frequency ω increases, β decreases. The blue shaded region highlights when the diffusion time over the rod area is less than the precession period. (inset) The reduced frequency at which $\beta = \theta/2$ as a function θ for simulated (red) and theory (green dash).

$$U = 2(N-1)\frac{\mu_o\mu^2}{4\pi r^3}(1 - 3(\hat{\boldsymbol{\mu}}\cdot\hat{\boldsymbol{r}})^2), \quad (3)$$

where N is the number of beads, μ_o is the magnetic constant, μ is the dipole magnitude, r is the distance between dipoles, and $\hat{\boldsymbol{r}}$ is the displacement vector. In a stiff chain, we take $\hat{\boldsymbol{r}} = \hat{\boldsymbol{n}}$ and the distance r between dipoles to be the size of the particle σ. Taking the derivative with respect to the degree of freedom α yields

$$\frac{\partial U}{\partial \alpha} = \frac{-3N\mu_o\mu^2}{\pi\sigma^3}(\sin^2\beta\sin^2\theta\sin\phi(\cot\beta\cot\theta + \cos\phi)). \quad (4)$$

Note that in the static-field limit, $\phi \to 0$ and $\beta \to \theta$, this expression results in no torque on the rod ($\partial U/\partial\alpha \to 0$), as expected.

The rod of length l is coated in a passive, non-magnetic layer making the diameter $d > \sigma$. The dissipation function acting on the rod is approximated as the sum of friction elements along the rod,

$$P = \frac{1}{2}\sum_{i}^{l/2} 2kv_i^2, \quad (5)$$

where the sum over each term considers the velocity v_i at each element given the friction coefficient $k = 3\pi\eta d$, where η is the dynamic viscosity of the fluid. There is a total of l/d number of friction elements each with diameter d. In Eq. 5, we see that the sum P along the whole rod l is equal to twice the sum in one direction along the rod starting from the center of precession. The velocity of each element i is $v_i = u_i\,\omega\sin\beta$, where u_i is the distance along the rod from the center of precession. The distance u increments by $d/2$ because the center of mass (the stationary point during precession) shifts by this amount. That is, the rod precesses around its center element when l/d is even

or precesses between two elements when l/d is odd. Note that the number of drag elements is not the same as the number of superparamagnetic beads N. For calculating $\sum v_i^2$, we can replace the terms in u^2 with integers by multiplication $(2u_i)^2/4$ allowing us to replace the sum with an expression for the sum of all integers up to l/d, $\sum(2u_i)^2 = (2l/d+1)(l/d+1)(l/d)/6$. This leads to the equation for the drag torque

$$\frac{\partial P}{\partial \dot{\alpha}} = \frac{\pi}{4}\eta\sigma\omega d^3\left(2\frac{l}{d}+1\right)\left(\frac{l}{d}+1\right)\left(\frac{l}{d}\right)\sin^2\beta. \qquad (6)$$

We see that when l/d goes to zero (a sphere), so does the drag torque. The drag torque can be modified by employing a correction factor $k' = kf$ derived by Lamb[31] for a cylinder, where $f = (1/2 - \gamma - \ln Re/8)^{-1}$, where γ is Euler's constant, and $Re = v_i d/\nu$ is the Reynolds number, where ν is the kinematic viscosity. Plugging in our expressions in Eq. 4 and Eq. 6 into Eq. 2 leads to the relation,

$$\Omega\sin^2\theta\sin\phi(\cot\beta\cot\theta + \cos\phi) + \omega = 0, \qquad (7)$$

where $\Omega = 12N\mu_o\mu^2/\eta\pi^2\sigma^3 d^3(l/d)^3$ for long rods ($l/d \gg 1$). The magnetoviscous ratio Ω is a characteristic frequency that depends on the strength of the magnetic energy ($\sim N\mu_o\mu^2/\sigma^3$) compared to the viscous drag ($\sim\eta d^3(l/d)^3$) and can be thought of as a characteristic "response" frequency of the rod in a dynamic magnetic field. Solving for β, we obtain our final expression for the rod precession angle,

$$\beta = \cot^{-1}\left(\frac{2\ \omega'\csc\phi}{\sqrt{3}\ \sin 2\theta} - \cos\phi\tan\theta\right). \qquad (8)$$

The reduced field frequency $\omega' = \omega\sqrt{3}/\Omega$ defines the relationship between the rod response time and the field precession period. While ω' is a magnetoviscous parameter,[30] leaving it as reduced frequency intuitively reflects its role as a scaled frequency. Therefore, it is easy to see the β curve for a particular θ in Fig. 1a becomes centered at 1 when plotting against ω'. The reduced field frequency can be rewritten in terms of a set of dimensionless constants,

$$\omega' = \frac{1}{72\sqrt{3}}\frac{\ln\left(\frac{l}{d}+1\right)+C}{R^4\Gamma D'}, \qquad (9)$$

where R is the thickness ratio d/σ, the magnetic coupling constant $\Gamma = \mu_o\mu^2/2\pi d^3 k_B T$, where k_B is the Boltzmann constant, and T is the absolute temperature, $D' = D/\omega A$ is the relative diffusion constant relating the diffusion timescale over the rod area $A = ld$ to the field precession period. The $\ln(l/d+1)+C$ terms relate to the diffusion $D = k_B T(\ln(l/d+1)+C)/3\pi\eta l$, where $C \approx 0.312$ for sufficiently long rods ($< 5\%$ error for $l/d > 4$).[32]

To find the expression for ϕ, we solve Eq. 8 in the slow field limit. Under a pseudo-static field, the rod will maintain alignment with the field direction. This limit implies $\beta \to \theta$ and that the lag is very small leading to $\cos\phi \to 1$. We obtain $\phi = \tan^{-1}(\omega/[(\Omega-\omega)(\Omega+\omega)]) \approx \tan^{-1}(\omega'/\sqrt{3})$.

Eq. 8 shows that there is a well-defined intermediate frequency at which $\beta = \theta/2$. If we set this condition for β and solve for ω, assuming real solutions with $\omega > 0$, we can expand a power series around $\cos\theta = 1$ to obtain

$$\omega'_{\theta/2} = 1 + \frac{5}{\sqrt{3}}(\cos\theta - 1). \qquad (10)$$

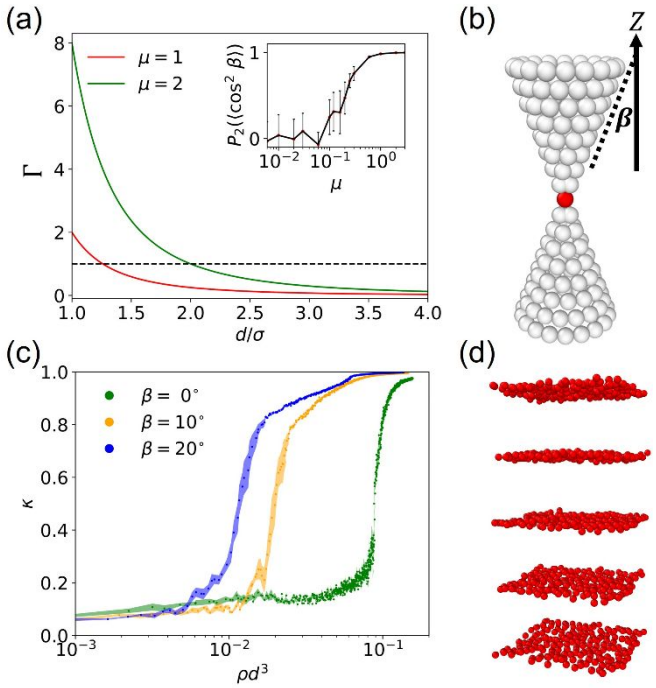

Fig. 2 (a) The magnetic coupling $\Gamma(\sim 1/d^3)$ decreases as the distance between dipoles ($\mu = 1$ (red) and 2 (green)) increases. (a, inset) The orientational order of magnetic rods as μ increases with error bars representing one standard error in the order. (b) Steric MD model, that assumes small Γ, where the red bead is the centre of precession for a rod ($l/d = 8$) and the white beads fill the skin of a double-cone matching the rod precession angle β. (c) The smectic order of the steric model at various precession angles showing how increasing β decreases the transition density. Shaded areas represent one standard error. (d) Steric model in the smectic phase; for clarity, only the red centre beads are shown.

2.2 Magnetic MD Model

We represent a coated, superparamagnetic rod as a linear chain of magnetic beads of diameter σ that are covered evenly in a non-magnetic layer with thickness $d - \sigma = 2\sigma$. The rod moves rigidly in response to a magnetic field. We simulate a system of rods suspended in solution with a constant density ρ under isothermal and isochoric conditions (the NVT ensemble). Time is integrated with a step of $0.002\ \tau$, where the unit of time $\tau = \sigma\sqrt{m/\epsilon}$, where m is the mass of one magnetic bead. The temperature of the system is maintained by the Langevin method.[33] The temperature is set such that the thermal energy $k_B T$ is equal to the energy unit ϵ and the damping coefficient is $5\ m/\tau$.

The potential energy of the system is a sum of the magnetic and hard-core interactions. The dipole moment $\boldsymbol{\mu}$, at the centre of each bead is oriented in the direction of field $\boldsymbol{H}$, as described

in Section 2.1. The magnitude of the dipole moments μ are identical and have units of $\sqrt{\mu_o/4\pi\sigma^3\epsilon}$. The potential energy is the sum of all the dipole-dipole interactions for each bead within a cut off distance of 5σ. The potential energy of one dipole pair is $U_{ij} = \sum_i^M \sum_j^{M'} \frac{\mu_o \mu^2}{4\pi r^3}\left(1 - 3(\hat{\boldsymbol{\mu}} \cdot \hat{\mathbf{r}}_{ij})^2\right)$, where M is the total number of beads in the system, and $\hat{\mathbf{r}}_{ij}$ is the displace vector between beads i and j. Rod collisions are purely repulsive and add to the total potential energy using the defined by the Weeks-Chandler-Andersen (WCA) potential,[34] where the distance parameter σ_{WCA} is set to the total rod thickness d.

The nematic and smectic phases were quantified by calculating their respective order parameters. The orientational information in a collection of symmetric rods (or molecules) can be determined using the order tensor,[35]

$$Q = \frac{1}{N}\sum_i^{N_i}\left(\hat{u}_{i,\alpha}\hat{u}_{i,\beta} - \frac{\delta_{\alpha\beta}}{3}\right) \quad (11)$$

where Q is a second rank tensor, N is the number of rods, $\hat{u}_i$ is the unit orientation vector of rod i, and α and β are the Cartesian coordinates x, y, and z. It is usually assumed that Q is calculated over a small macroscopic volume, which is represented by our simulated system. The nematic director $\hat{\boldsymbol{n}}$ corresponds to the eigenvector of Q with the largest eigenvalue. The smectic order considers the location of the center of each rod, $\boldsymbol{r}$

$$\kappa = \max_d \left|\left\langle \exp\left(2\pi i \frac{\boldsymbol{r}\cdot\hat{\boldsymbol{n}}}{d}\right)\right\rangle\right|, \quad (12)$$

where the layer spacing d is chosen to maximize the order κ. A practical method of extracting smectic order parameter from experiments is to use diffusion data.[36]

The precession around the z-axis implies that, if the smectic state is present, the length of the box in the z-direction L_z must be an integer number of layers n. We don't know the layer thickness *a priori* but it will be a function of the rod length $f_0(l)$. There will be a mismatch in the lengths L_z and $nf_0(l)$. This difference will be distributed over all layers $\delta = L_z/n - f_0(l)$. If δ is small, then $L_z/n \approx f_0(l)$. We can inform how long to make L_z by using the maximum possible value for $\delta_{max} = l/2$. By assuming that $f_0(l) \to l = 24\sigma$ for small β, we determine that the maximum error in layer spacing over $n = 50$ layers is 0.24σ. The real number of layers we observe is 50 ± 1. The box contains $9{,}800$ rods that are initialized with a random position and orientation. The density begins at $d^3\rho = 0.01$ and is slowly increased at a rate of $3.125 \times 10^{-6} d^3\rho/\tau$ by isotropically shrinking the x-y area.

2.3 Purely steric "strong precession" MD model

In the case of low magnetic coupling between rods, we explore a model where the essential physics of the system can be captured without explicit dipole-dipole calculations. Assumptions for this purely steric model are (1) a strong field to maintain the orientation of the rods against Brownian motion, (2) a sufficiently thick passive layer to maintain low magnetic coupling between rods (large R, small Γ), (3) a precession period much faster than the rod diffusion time (small D'), and (4) a rod precession angle β not suppressed by collisions (low $d^3\rho$).

The first and second assumptions allow us to ignore dipole-dipole calculations and rotation dynamics. We assume that the rods will always point in the direction of the precessing field. Regardless of how strong the dipole interactions are to meet this condition, the magnetic coupling remains small because the nonmagnetic layer is sufficiently thick (Fig. 2a).

The third assumption relates to how the space swept out by a precessing rod over one precession period; that is, distribute repulsive particles along the skin of a double-cone to create an implicit precession. Superparamagnetic rods of identical lengths are in-phase while precessing, meaning that the "precessing" white particles (Fig. 2b) do not interact with other white particles. Repulsive interaction is only felt between the central red particle and all other particles. Due to this interaction, the rod must extend l distance away from the center to represent the correct l/d. The density of the white particles is set to $\sim 1/\sigma^2$. The fast field or slow diffusion assumption is distinct from field that is precessing in the limit of infinite precession speed, which we have describe previously.[37-39] In that case, the field was fast compared to the rod (or chain) response time, analogous to $1/\Omega$. We model it as a rigid body and, since it follows the field, rigid body rotation is restricted.

Assumption (4) depends on dilute conditions. Even in the absence of a magnetic field, increasing rod density, forces the alignment of the rods. This necessarily suppresses β until, at the high density limit, $\beta \to 0$. However, simulations suggest that there is little deviation in β during the nematic-smectic transition, which we show later on in Fig 3.

Based on these conditions we have developed a purely repulsive model to represent an ensemble of precessing rods. The rods are composed of two types of particles: red and white, as shown in Fig. 2b. The repulsive potential between red-red is defined by the WCA potential, as mentioned in Section 2.2. However, the red-white potential is a soft-core potential[40] reflecting the finite strength of the precession barrier preventing rods from freely diffusing. This potential is given as

$$U_{rw} = 4\epsilon\lambda^b\left[\frac{1}{w^2} - \frac{1}{w}\right], \quad (13)$$

Where the activation parameter $\lambda = 0.1$, $b = 1$, $w = p(1-\lambda)^2 + (r/d)^6$, where $p = 1/2$, and r is the bead-bead distance below the cut off $r = 1.1d$ when the potential reaches zero ($U_{rw}(r = 1.1d) = 0$). These parameters result in a soft core barrier of $2\ k_BT$.

The simulation begins with 1000 rods randomly distributed in a cubic box with periodic boundaries. We integrate time using an NPT ensemble using a time step of $0.001\ \tau$. Like the magnetic MD model, the temperature is controlled by Langevin dynamics and the pressure is maintained using the Nosé-Hoover algorithm.[41] We apply a slow pressure ramp to maintain quasi-constant pressure beginning at $P\sigma^3/\epsilon = 0.1$ to 1.0, encompassing the relevant range of densities in which the nematic-smectic transition occurs. The box axes are allowed to relax anisotropically with the x and y axes coupled for visual convenience. The transition from nematic to smectic is defined by the inflection point (i.e. half max smectic order) averaged over 5 simulations.

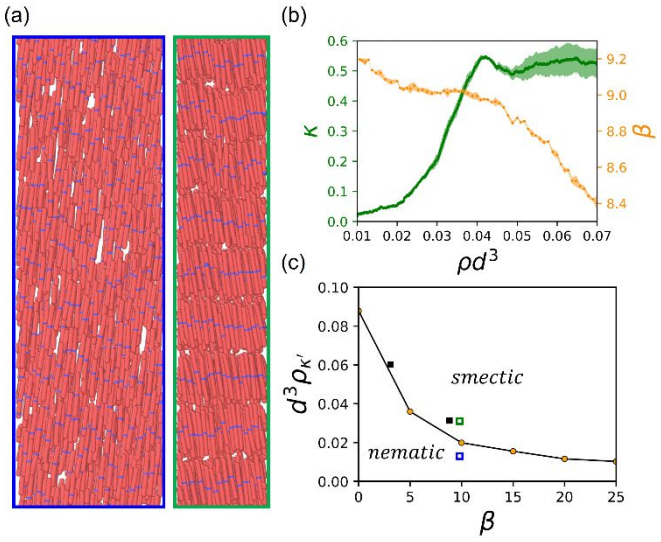

Fig. 3 (a) Magnetic MD model below (left) and above (right) the nematic-smectic transition ($\theta = 20°$, $\omega' = 0.2$). (b) The smectic order κ and rod angle β for the magnetic MD model as the system density ρd^3 increases. (c) The phase diagram separating the nematic and smectic regions. The data points represent the density at half of the maximum smectic order $d^3\rho_{\kappa'}$. The orange data is the strong precession model and the black squares denote the observed transition from the magnetic MD model, with green and blue highlight snapshots from (a).

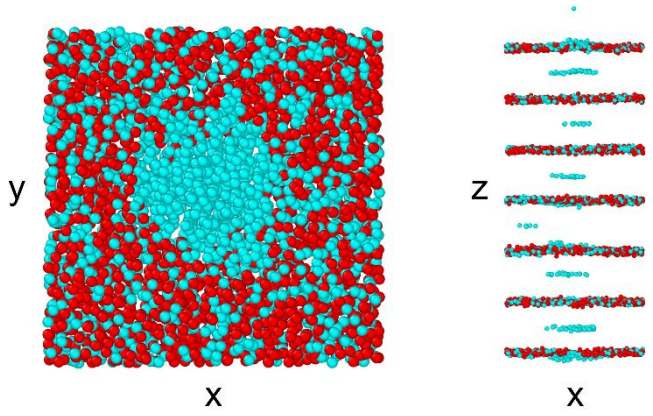

Fig. 4 A (50% cyan $l/d = 4$: 50% red $l/d = 8$) binary mixture of rods in the smectic regime, centres shown for clarity.

For the binary mixtures, the same method as the single component simulations was applied with 3,456 rods, randomly distributed in an initially cubic box, (1:1 mixture of $l/d = 4$, $\beta = 29°$, $\sigma = 0.97$; $l/d = 8$, $\beta = 12°$, $\sigma = 1.0$). This combination is consistent with rods under a field precessing at $\theta = 40°$ and $\omega = 0.14/\tau$. The difference in their l/d and σ ($\sim\mu^{1/3}$) alone result in a different angle of precession. In this case, the implicit magnetic coupling remains below one ($\Gamma = 0.06$ and 0.07 for the $l/d = 4$ and $l/d = 8$, respectively). In addition, the reduced diffusion is also small ($D' = 2 \times 10^{-3}$ and 10^{-3} for the $l/d = 4$ and $l/d = 8$, respectively).

3 Results and Discussion

The viscous drag on a rotating superparamagnetic rod significantly impacts its motion in precessing magnetic fields. The rod's precession angle β and azimuthal phase lag ϕ must result in a magnetic torque (Eq. 4) that balances the drag torque (Eq. 6). We show in Fig. 1b the curve describing the rod precession angle β as a function of the field precession frequency ω (for $\theta = 20°$ and $50°$). In the static field limit (small ω), the rod precession matches the field angle $\beta = \theta$. As ω increases, $\beta \to 0$ according to Eq. 8, having good agreement with MD simulations.

To uniquely determine β, two variables must be known: θ and the reduced field frequency ω'. This dimensionless parameter from Eq. 9 rescales ω relative to the magnetoviscous response frequency of the rod, and otherwise acts conceptually identical to the field frequency. In Eq. 8, we theoretically derive $\beta(\theta,\omega')$ and produce a curve (Fig. 1b, dashed line) nearly identical to that of MD simulations (Fig. 1b, solid line).

The inflection point in the $\beta(\theta,\omega')$ curve is a characteristic frequency at which $\beta = \theta/2$. In Eq. 10, we expand Eq. 8 in a power series to obtain a simple relationship to predict the characteristic frequency $\omega'_{\theta/2}$, which remains accurate for small precession angles (Fig. 1b, inset). This frequency is well-defined at experimentally realizable intermediate frequencies and is useful as a way of describing the system's precession properties, such as the reduced diffusion constant $D'(\omega)$ from Eq. 9.

Precession induced properties are dependent on $D' \ll 1$ because this is the regime where the precession period is shorter than the diffusion time across the precession barrier. In Fig. 1b, we shade the region where the rods diffuse faster than the field precesses. Diffusion time decreases with decreasing temperature; however, the temperature cannot be arbitrarily lowered because the magnetic coupling $\Gamma \sim 1/\mathrm{T}$ must also be less than 1 to ensure thermal energy dominates over magnetic-induced effects.

We control the magnetic coupling by coating the rods with a non-magnetic layer. Increasing the distance between superparamagnetic dipoles rapidly decreases $\Gamma \sim 1/d^3$. The magnetic coupling can also be decreased by weakening the magnetic field, but doing so may collapse orientational (nematic) order[42] (Fig. 2a, inset). From Fig 2a, we see that for any reasonable magnitude for the dipole moment μ, the magnetic coupling Γ quickly decays to below 1 when the thickness of the passive layer is on the order of the magnetic particle diameter. For our model, we consider rods coated by a σ thick passive layer, where σ is the diameter of the magnetic nanoparticles, for a total rod diameter of 3σ.

With the conditions $D' \ll 1$ and $\Gamma \ll 1$ met, we introduce the purely steric "strong precession" model, described in detail in Section 2.3. The skin of a double-cone, swept out by the rod, is treated as a soft barrier to the centres of other rods (Fig. 2b).

Since, the rods are in-phase, the beads in the white "double-cone" beads can overlap with white beads in other rods. This model specifies β as a constant, which implicitly sets θ and ω' without needing to perform dipole-dipole calculations. In Fig. 2c, we show that the transition to the layered (smectic) phase occurs at a lower density for larger precession angles. The transition is defined by the density at which the system reaches half the maximum smectic order. The centres of the rods in the smectic phase can be seen in Fig. 2d. Obscuring the white beads allows us to see the disordered layers that indicate a small magnetic coupling regime.

We observe the same density suppression for the nematic-smectic transition using the full magnetic MD model. The sharpness of the transition and the maximum smectic order depends on the strength of the precession barrier. As the system density increases, the collision frequency between rods increases and results in a continuous transition to the smectic phase, given a constant β (Fig 3b). The magnetic MD model is not in the strong precession limit, therefore, the density required to induce the nematic-smectic transition is slightly higher than the steric model (Fig. 3c). This indicates that the precession barrier is easier to diffuse across, meaning that different temperatures can be modelled by adjusting the energy barrier in the steric model. Finally we should note that, the MD model validates the steric model's assumption that the precession angle does not change by showing that the transition occurs over densities with negligible changes to β.

In Fig. 4, we use for the steric model to investigate the behaviour of binary mixtures of different length rods, $l/d = 4$ (cyan) and 8 (red), where the system would normally be too large to investigate using the magnetic mode. We see synchronization-driven phase separation occurring due to the steric repulsion of incompatibly precessing rods.[43] We observe two phases: a mixed phase and a phase rich in short rods. The short rods precess at a larger angle and therefore the steric cost of the mixed phase decreases more with a short rod rich phase than a long rod rich phase. Full segregation does not occur due to the entropy of the diffusing rods. The presence of the interstitial layers suggests possible consequence of local alignment. In the absence of sufficient fluctuations or shear forces, layers may stabilize defects such as two regions of the long-rod phase offset by one short-rod layer.

4 Conclusions

In summary, the density at which the nematic-to-smectic transition occurs in a system of precessing rods decreases with increasing precession angle. We show this effect using a purely steric molecular dynamics model and validate it in a superparamagnetic system. Systems with rods of disparate lengths will phase separate and can form stable defects in the smectic layers. Future work is needed to define the phase boundaries present in systems of binary mixtures. We anticipate that a better understanding of liquid crystal phase transitions in dynamic magnetic fields will advance the design and control of liquid crystal-based devices.

Conflicts of interest

There are no conflicts to declare.

Acknowledgements

We thank the Sherman Fairchild Foundation for computational support. This research was supported by the Center for Bio-Inspired Energy Science, an Energy Frontier Research Center funded by the U.S. Department of Energy, Office of Science, Basic Energy Sciences under Award No. DE-SC0000989.

Notes and references

1 M. Wang and Y. Yin, *J. Am. Chem. Soc.,* 2016, **138**, 6315.
2 F. X. Redl, K.-S. Cho, C. B. Murray and S. O'Brien, *Nature*, 2003, **423**, 968.
3 K. Petcharoen and A. Sirivat, *Mater. Sci. Eng. C*, 2016, **61**, 312-323.
4 J. Liu, Y. Cai, Y. Deng, Z. Sun, D. Gu, B. Tu and D. Zhao, *Microporous Mesoporous Mater*., 2010, **130**, 26.
5 Y. Zhang, Q. Yue, M. M. Zagho, J. Zhang, A. A. Elzatahry, Y. Jiang, and Y. Deng, *ACS Appl. Mater. Interfaces*, 2019, **11**, 10356.
6 A. McMullen, M. M. Basagoiti, Z. Zeravcic, and J. Brujic, *Nature*, 2022, **610**, 502.
7 X. Wang, D. S. Miller, J. J. de Pablo, and N. L. Abbott, *Adv. Funct. Mater.*, 2014, **24**, 6219.
8 J. Shin, M. Kang, T. Tsai, C. Leal, P. V. Braun, D. G. Cahill, *ACS Macro. Lett.*, 2016, **5**, 955.
9 V. Rastogi, A. A. García, M. Marquez, and O. D. Velev, *Macromol. Rapid Commun.*, 2009, **31**, 190-195.
10 M. Chen, H. Cölfen and S. Polarz, *ACS Nano*, 2015, **9**, 6944.
11 S. S. Park, Z. J. Urbach, C. A. Brisbois, K. A. Parker, B. E. Partridge, T. Oh, V. P. Dravid, M. Olvera de la Cruz, C. A. Mirkin, *Adv. Mater*., 2020, **32**, 1906626.
12 L. Etgar, G. Leitus, L. Fradkin, Y. G. Assaraf, R. Tannenbaum and E. Lifshitz, *Chemphyschem*., 2009, **10**, 2235.
13 Z. Li, C. Qian, W. Xu, C. Zhu, Y. Yin, *Sci. Adv*., 2021, **7**, eabh1289.
14 T. Ding, K. Song, K. Clays and C.-H. Tung, *Langmuir*, 2010, **26**, 11544.
15 D. Andrienko, J. Mol. Liq., 2018, **267**, 520.
16 P. G. de Gennes, and J. Prost, *The physics of liquid crystals*, Oxford University Press, Oxford, 1993.
17 M. A. Gharbi, I. B. Liu, Y. Luo, F. Serra, N. D. Bade, H.-N. Kim, Y. Xia, R. D. Kamien, S. Yang, and K. J. Stebe, 2015, *Langmuir*, **31**, 11135.
18 K. Hiraoka, P. Stein, and H. Finkelmann, *Macromol. Chem. Phys*., 2004, **205**, 48.
19 A. Sánchez-Ferrer and H. Finkelmann, *Mol. Cryst. Liq. Cryst*., 2009, **508**, 348.
20 J. Yoon, A. J. Baca, S.-I. Park, P. Elvikis, J. B. Geddes, L. Li, R. H. Kim, S. Wang, T.-H. Kim, M. J. Motala, B. Y. Ahn, E. B. Duoss, J. A. Lewis, R. G. Nuzzo, P. M. Ferreira, Y. Huang, A. Rockett and J. A. Rogers, *Nat. Mater.*, 2008, **7**, 907.
21 S. Hu, K. Dasbiswas, Z. Guo, T.-H. Tee, V. Thiagarajan, P. Hersen, T.-L. Chew, S. A. Safran, R. Zaidel-Bar, and A. D. Bershadsky, *Nat. Cell Biol.*, 2017, **19**, 133.
22 H. Hama, *J. Phys. Soc. Jpn*., 1985, **54**, 2204.
23 J. S. Andreu, J. Camacho and J. Faraudo, *Soft Matter*, 2011, **7**, 2336.
24 S. Y. Lee, and S. Yang, *Angew. Chem. Int. Ed.,* 2013, **52**, 8160.
25 W. H. Chong, L. K. Chin, R. L. S. Tan, H. Wang, A. Q. Liu, H. Chen, *Angew. Chem. Int. Ed*., 2013, **52**, 8570.

26 A.-H. Lu, E. L. Salabas and F. Schüth, *Angew. Chem. Int. Ed*., 2007, **46**, 1222.
27 W. H. Chong, L. K. Chin, R. L. S. Tan, H. Wong, A. Q. Liu, and H. Chen, *Angew. Chem. Int. Ed.*, 2013, **52**, 8570.
28 J. Cīmurs and A. Cēbers, *Phys. Rev. E*, 2013, **87**, 062318.
29 H. Goldstein, *Classical Mechanics*, 3rd Ed. (Addison-Wesley, Reading, MA, 2000), p. 24.
30 C. A. Brisbois and M. Olvera de la Cruz, *Phys. Rev. Res*., 2022, **4**, 023166.
31 H. Lamb, *Phil. Mag.*, 1911, **21**, 112.
32 A. Ortega and J. García de la Torre, *J. Chem. Phys.,* 2003, **119**, 9914.
33 T. Schneider and E. Stoll, *Phys. Rev. B*, 1978, **17**, 1302.
34 J. D. Weeks, D. Chandler and H. C. Andersen, *J. Chem. Phys*., 1971, **54**, 5237.
35 J. Vieillard-Baron, *Mol. Phys.*, 1974, 28, 809.
36 M. Cifelli, G. Cinacchi, and L. De Gaetani, *J. Chem. Phys*., 2006, **125**, 164912.
37 J. M. Dempster, P. Vázquez-Montejo and M. Olvera de la Cruz, *Phys. Rev. E*, 2017, **95**, 052606.
38 P. Vázquez-Montejo, J. M. Dempster and M. Olvera de la Cruz, *Phys. Rev. Mater.*, 2017, **1**, 064402.
39 C. A. Brisbois, M. Tasinkevych, P. Vázquez-Montejo and M. Olvera de la Cruz, *Proc. Natl. Acad. Sci. U.S.A.*, 2019, **116**, 2500.
40 T. C. Beutler, A. E. Mark, R. C. van Schaik, P. R. Gerber, and W. F. van Gunsteren, *Chem. Phys. Lett.*, 1994, **222**, 529.
41 W. Shinoda, M. Shiga, and M. Mikami, *Phys. Rev. B*, 2004, **69**, 134103.
42 A. R. Khokhlov and A. N. Semenov, *Macromolecules*, 1982, **15**, 1272.
43 G. Paulo and M. Tasinkevych, *Phys. Rev. E*, 2021, 104, 014204.